Petroleum Science 21 (2024) 1221–1230

Contents lists available at ScienceDirect

Petroleum Science

journal homepage: www.keaipublishing.com/en/journals/petroleum-science

Original Paper

The influences of perforating phase and bedding planes on the fracture deflection in laminated shale

Ming-Zhe Gu [a, b], Mao Sheng [a, b, *], Xiao-Ying Zhuang [c, **], Xin-Yi Li [c], Gen-Sheng Li [a, b]

[a] National Key Laboratory of Petroleum Resources and Engineering, China University of Petroleum, Beijing, 102249, China
[b] College of Petroleum Engineering, China University of Petroleum, Beijing, 102249, China
[c] College of Civil Engineering, Tongji University, Shanghai, 200092, China

ARTICLE INFO

Article history:
Received 14 February 2023
Received in revised form
17 October 2023
Accepted 18 October 2023
Available online 19 October 2023

Edited by Jia-Jia Fei

Keywords:
Shale
Propagation
Perforating
Bedding
Structure

ABSTRACT

The perforating phase leads to complex and diverse hydraulic fracture propagation behaviors in laminated shale formations. In this paper, a 2D high-speed imaging scheme which can capture the interaction between perforating phase and natural shale bedding planes was proposed. The phase field method was used to simulate the same conditions as in the experiment for verification and hydraulic fracture propagation mechanism under the competition of perforating phase and bedding planes was discussed. The results indicate that the bedding planes appear to be no influence on fracture propagation while the perforating phase is perpendicular to the bedding planes, and the fracture propagates along the perforating phase without deflection. When the perforating phase algins with the bedding planes, the fracture initiation pressure reserves the lowest value, and no deflection occurs during fracture propagation. When the perforating phase is the angle 45°, 60° and 75° of bedding planes, the bedding planes begin to play a key role on the fracture deflection. The maximum deflection degree is reached at the perforating phase of 75°. Numerical simulation provides evidence that the existence of shale bedding planes is not exactly equivalent to anisotropy for fracture propagation and the difference of mechanical properties between different shale layers is the fundamental reason for fracture deflection. The findings help to understand the intrinsic characteristics of shale and provide a theoretical basis for the optimization design of field perforation parameters.

1. Introduction

Multi-cluster perforation is one of key procedures of the plug and perforation fracturing (Cai et al., 2019; Michael and Gupta, 2020). The perforating phase has been confirmed to be a significant influence on laminated shale hydraulic fracture propagation (Abass et al., 1996; Bai et al., 2020). Therefore, understanding the hydraulic fracture propagation and their morphology under the influence of perforating phase and bedding planes, is necessary to enhance the efficiency of mass hydraulic fracturing in shale gas reservoir.

The influence of perforation has been studied by many authors. Daneshy (1973) found that the increase of perforation diameter can effectively reduce the formation tensile strength by theoretical analysis and physical experiments as early as 1973. Lei et al. (2015) found out that the presence of perforation can significantly reduce the breakdown pressure and the increase of perforation depth is conducive to fracture initiation and propagation. Furthermore, by varying the horizontal stress ratio, Liu et al. (2016) and Zhang et al. (2018) observed multiple types of fracture patterns under different perforation parameters: a single flat, spiral-shaped, multiple-main or network fractures.

Some progress has been made on the influence of bedding planes on fracture propagation. A complex fracture geometry with tortuous propagation trajectories is created in both tensile and shear fracture modes because of the activation of shale bedding structures (Daneshy, 2003). Laboratory experiments have observed several typical propagation modes of fracture: penetration, deflection and arrest (Hou et al., 2018; Wang et al., 2021; He et al., 2022; Zhang et al., 2023). In order to better understand the complex

* Corresponding author. National Key Laboratory of Petroleum Resources and Engineering, China University of Petroleum, Beijing, 102249, China.
** Corresponding author.
E-mail addresses: shengmao@cup.edu.cn (M. Sheng), zhuang@iop.uni-hannover.de (X.-Y. Zhuang).

https://doi.org/10.1016/j.petsci.2023.10.015

propagation behaviors of hydraulic fracture in the rock sample after fracturing, Acoustic Emission (AE) and Computed Tomography (CT) scan monitoring techniques have been widely used. Wu et al. (2022) concluded that the existence of layered structure made the formation of hydraulic fractures no longer simple tensile action, and the slip of fractures could not be ignored through AE monitoring. Guo et al. (2014) obtained the fracture propagation pattern of horizontal shale wells by observing the experimental cores under different parameter conditions by high-energy scanning. Furthermore, the typical hydraulic fracture propagation behaviors have been confirmed by several numerical simulation works (Zou et al., 2018; Liu et al., 2020; Cong et al., 2022; Zhang et al., 2022). Although the complex fracture propagation behaviors influenced by perforation parameters and bedding plane structure have been identified, yet the high-speed imaging of hydraulic fracture propagation in bedding shale samples with perforation and its intrinsic reasons have rarely been addressed.

In this paper, a 2D high-speed imaging scheme for hydraulic fracturing test was used to understand the effect of perforating phase and bedding planes on hydraulic fracture propagation. High resolution images and image processing technology can directly monitor and quantify the fracture propagation in experiments. Furthermore, numerical simulations consistent with experimental conditions were also used to gain further insight into the fracture propagation mechanism of shale hydraulic fracturing under different perforating phases. Results indicate that the perforating phase angle plays an important role on fracture propagation along the weak bedding planes or penetration into the matrix. Moreover, the mechanical difference between layers is the fundamental reason for the different deflection angles of fracture propagation.

2. Materials and methods

2.1. Material properties and sample preparation

The natural shale samples with bedding planes clearly visible for this study were taken from outcrops of the Lower Silurian Longmaxi Formation, Sichuan Basin, China. And the typical shale samples selected for the experiment contain 150 to 200 layers per 200 mm length as shown in Fig. 1. Their mineral compositions and contents interpreted from X-ray diffraction technique were listed in Table 1, which proved that the samples are the classical shallow black shale containing much quartz, dolomite, clay minerals, etc. Through a large number of rock mechanical tests on shale with parallel and vertical bedding planes as shown in Table A1, the mechanical parameters E_1, E_2, ν_{12} and ν_{23} were determined to be 21.1 GPa, 15.2 GPa, 0.19, 0.26 respectively.

The plate samples (100 mm length, 100 mm width, and 20 mm height) from the same block for each type of shale without any obvious fractures or other imperfections were all cored by the waterless wire cutting technique. Therefore, all samples have roughly the same mechanical properties such as strength, modulus, Poisson ratio, etc. The bedding planes of the samples were parallel to the direction of formation deposition. A 23 mm diameter injection hole was used for hydraulic fracturing, while 20° symmetrical notches, i.e. 5.5 mm long and 20 mm high, were opened on both sides so that the hydraulic fractures initiate preferentially in this direction. The wellbore was cemented into the center of the injection hole. Fine polishing was conducted to ensure sample surface are parallel within 100 μm or less which makes the contact stress on the interface uniform. Thin, soft transparent adhesive were spread evenly over the surface of the samples, and stood for 48 h to prevent fracturing fluid leakage. β is the angle between the bedding plane and the notch center line, taking values from 0° to 90°, known as the perforating phase angle. Notches of natural shale samples in different directions were used to simulate different perforating phases in real shale formations. As shown in Fig. 2, five perforating phase angles namely, $\beta = 0°$, 45°, 60°, 75°, and 90° respectively, were setup in the experiments to study the influences of perforating phase and bedding planes on the fracture deflection in laminated shale.

2.2. Experimental design

A 2D plane strain high-speed imaging scheme for hydraulic fracturing test was proposed without consideration of in-situ stress as shown in Fig. 3. The pressure curves were measured by a syringe pump. The maximum injection pressure is 50 MPa with the accuracy of ±0.1 MPa and the maximum injection rate is 50 mL/min. At the beginning of the experiment, the high-speed camera was placed directly in front of the sample at a distance of 80 cm. The LED light sources were placed on both sides of the sample 20 cm away to ensure that the captured images were clear and sharp. During the entire experiment process, the fracture propagation behaviors were recorded by a high-speed camera (1280 × 720 pixels) at 240 frames/sec. At the end of the experiment, the still keyframes of the

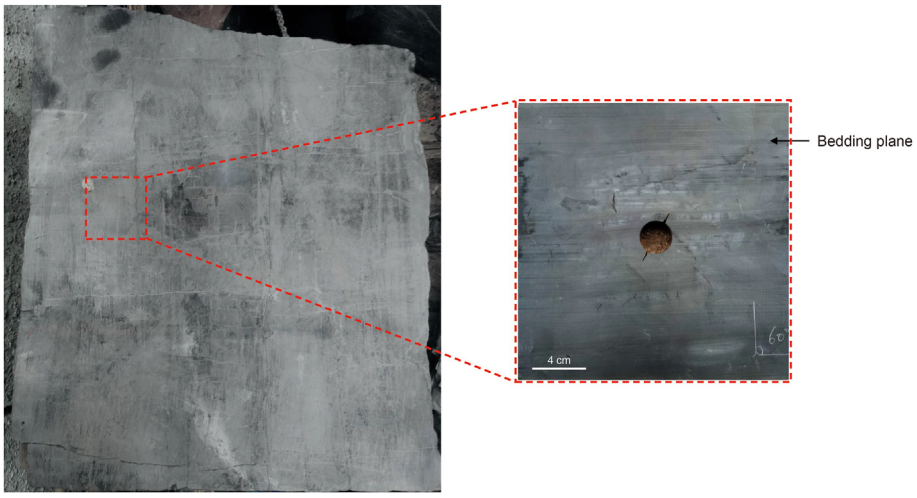

Fig. 1. Natural shale samples with bedding planes clearly visible.

Table 1
Mineral compositions of tested shale.

Mineral	Quartz	Feldspar	Calcite	Dolomite	Pyrite	Clay	Anhydrite
Weight percent, wt%	37.6	1.2	11.9	27.6	3.4	16.8	1.5

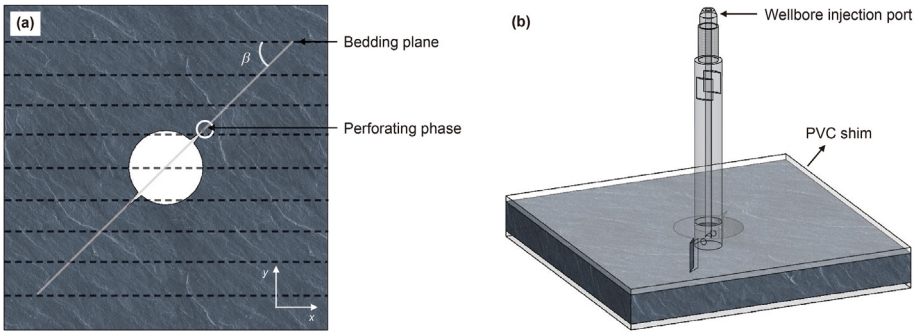

Fig. 2. Shale sample (**a**) and cementing seal (**b**) for hydraulic fracturing test.

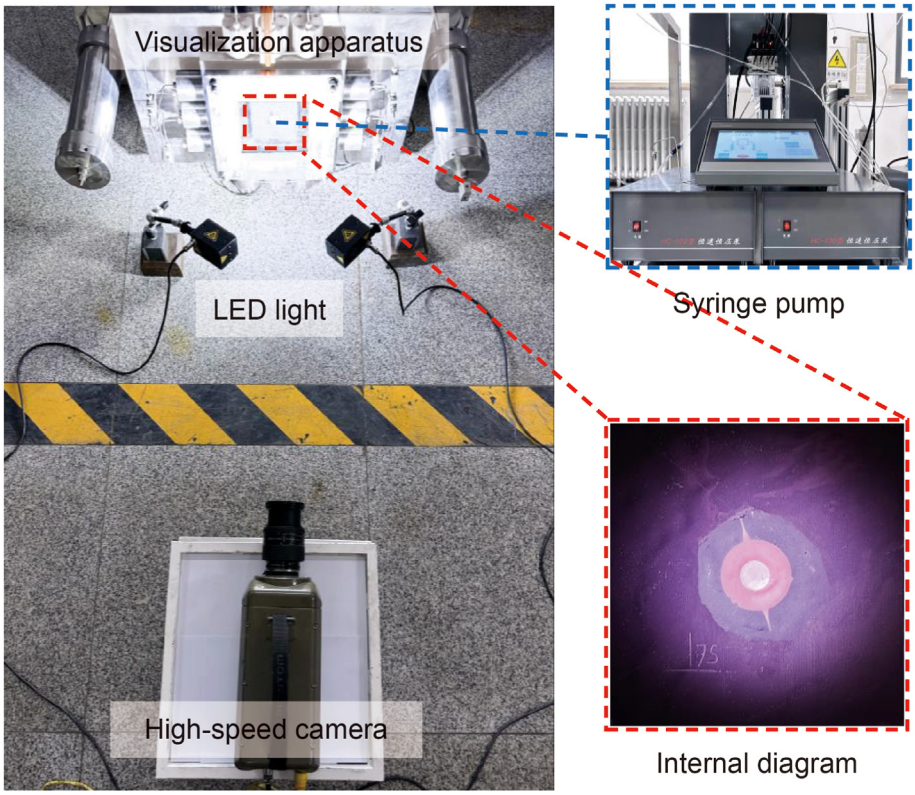

Fig. 3. Ongoing laboratory imaging of 2D hydraulic fracturing test.

fracturing process were extracted from the recorded video. The images were binarized by ImageJ to achieve accurate positioning of fracture propagation at each moment. Moreover, the experimental results can be directly verified with the 2D numerical model of hydraulic fracture propagation. Fig. 4 contains an overall view of the apparatus. The key to the success of the test is the sealing of the sample and the experimental setup. Two soft transparent PVC shims were utilized as sealing materials to be compacted on the surface of the sample respectively to resist the pressure of fracturing fluid, thus effectively reducing the probability of fluid leakage onto the sample surface during the tests.

Fig. 5 shows the layout of the experimental setup. 1 MPa pressure was applied in the Z direction to ensure that the PVC shims were closely fitted with the shale sample, and the fracture propagation of shale without in-situ stress is simulated without applying other directional stresses. The tested fracturing fluid is water with a viscosity of 1 mPa ·s. To ensure that the experimental parameters correspond to the field scale, the published laboratory data (Bunger and Detournay, 2008; Lu et al., 2022) and the typical field fracturing situations for shale formations were collected. Based on the similarity criterion proposed by Detournay (2016), the dimensionless parameters of fracture evolution corresponding to our experiments

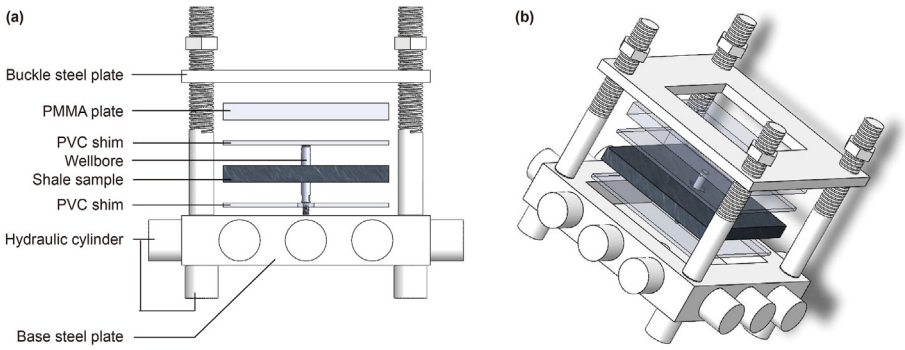

Fig. 4. Front (**a**) and side (**b**) view of 2D hydraulic fracturing visualization apparatus.

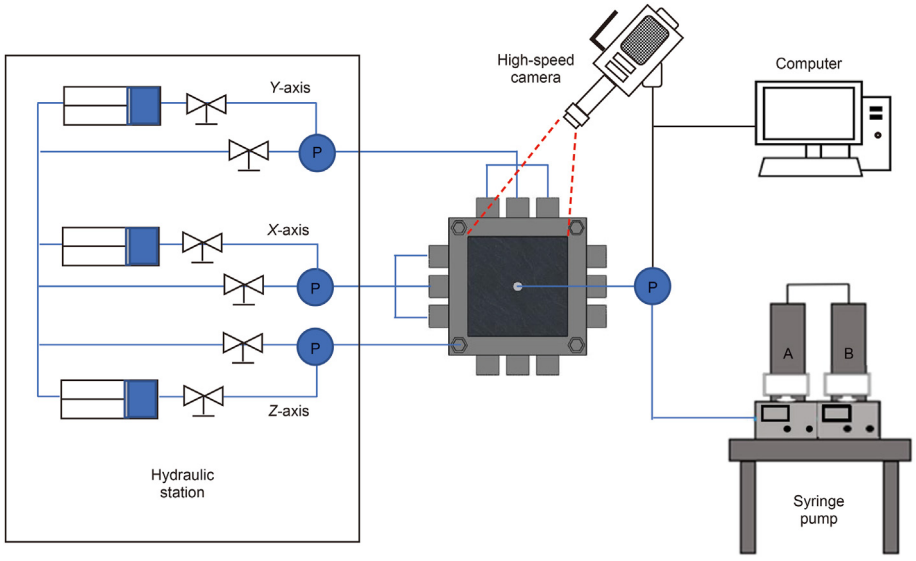

Fig. 5. Layout of the experimental setup.

and collected data were calculated as shown in Table A2. The low-viscosity fracturing fluid with a viscosity of 1 mPa·s and displacement of 1 m^3/min was selected under field conditions, and the injection rate of this experiment was determined to be 20 mL/min. The syringe pump was in constant speed mode and continued to inject until sample failure and all the procedures were performed at 28 °C.

2.3. Numerical simulation for experimental schemes

As a popular method widely implemented in hydraulic fracturing research, phase field method has obvious advantages (Zhuang et al., 2023). By introducing a phase field variable φ ($\varphi = 0$ and $\varphi = 1$ respectively represent intact and fully broken materials), the fracture model can be described by continuous functions without introducing discontinuity. In addition, the multi-field fracture propagation is transformed into a problem of solving a partial differential equation system (Francfort and Marigo, 1998).

As shown in Fig. 6, the calculation domain is a two-dimensional rock with internal fractures, which are denoted as Ω and Γ, respectively. The boundary of the calculation domain is marked as $\partial\Omega$, where the time-dependent Dirichlet boundary conditions $\boldsymbol{u}^*(\boldsymbol{x}, t)$ and the Neumann condition $\boldsymbol{t}^*(\boldsymbol{x}, t)$ must be satisfied on $\partial\Omega_u$ and $\partial\Omega_t$, respectively. Note that $\boldsymbol{x}$ is the position vector. On this basis, through a series of mathematics deductions, the governing equations of the hydraulic fracture propagation problem can be obtained. More details on isotropic and transversely isotropic media can be referred to Zhou et al. (2018) and Zhou and Zhuang (2020).

In order to gain further insight into the fracture propagation behavior in laminated shale, a 2D numerical model which was constructed with the same size and physical properties of the laboratory samples was carried out to investigate experimental results. As shown in Fig. 7, a total of three different rock matrices, isotropic, transversely isotropic, and multilayer rock, were designed to characterize the structural and mechanical properties of shale. The third of these matrices can still be considered as transversely isotropic from a macroscopic point of view.

Based on the phase field method, the fluid driven fracture propagation in different media due to increased fluid pressure on pre-existing notches was investigated (Zhou et al., 2018). The geometry and boundary conditions of the models are shown in Fig. 7 which were consistent with the experiments. All the outer boundaries were fixed for the displacement field. Linear triangular cells were used for mesh division in all numerical simulations and the maximum size is set as $h = 0.5$ mm. All rock mechanical parameters in numerical calculation were obtained by mechanical testing of shale samples which were similar to the previous fracturing experiments. A total of five perforating phase angles which were consistent with above experiments were simulated with

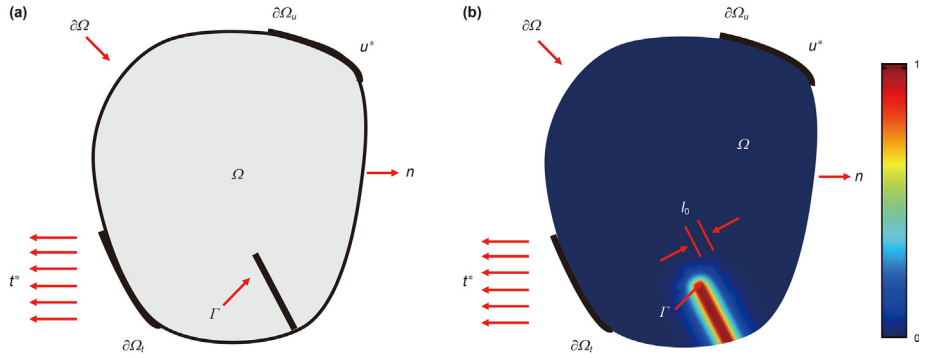

Fig. 6. Phase field representation of the (**a**) sharp fracture and (**b**) diffusive fracture.

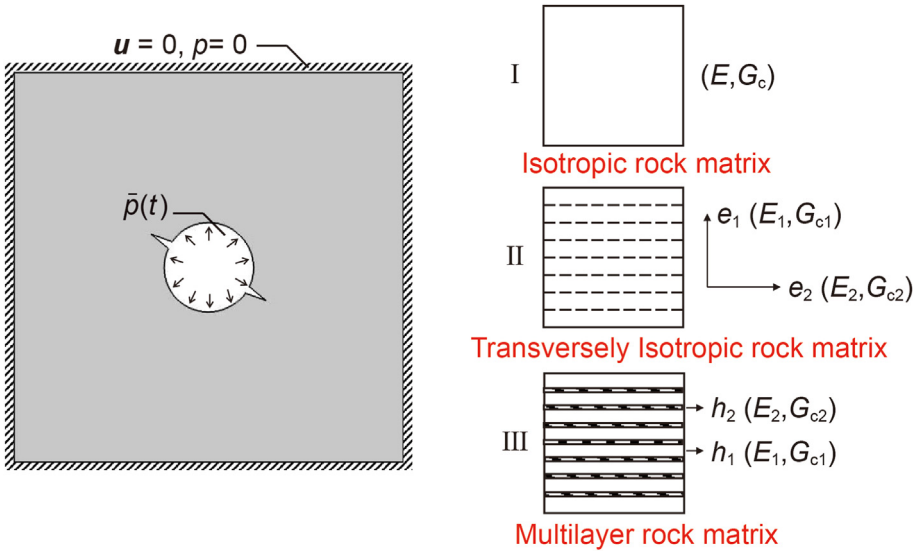

Fig. 7. Geometry and boundary conditions for different rock matrices subjected to internal fluid pressure.

other parameters unchanged. The fluid pressure on the notch surface is $p = 5\times10^4$ Pa/s. In addition, the mechanical parameters that characterize the properties of different rock matrices for calculation are listed in Table 2 (Zhou and Zhuang, 2020).

3. Results and discussion

3.1. Influence of perforating phase angle on fracture trajectory

Fig. 8 shows the hydraulic fracture initial and final propagation morphology in laminated shale at five perforating phases. Fig. 9 shows the degree to which different shale propagations deflect from the original perforating phase. All the shale samples were initiated from one side of the original perforating phase and propagated to the boundary within 1 s. When $\beta = 0°$ and 90°, fractures initiated along the original perforating phase and propagated without deflection. The fracture propagation trajectories coincide with the trajectory of type I fracture in isotropic medium (Li et al., 2013). However, compared with other perforating phase angles, it is found that the perforating phase angle has a significant influence on the direction of fracture propagation. When $\beta = 45°$, 60°, and 75°, fractures propagated obviously deflect from the original perforating phase and the tendency of fracture deflection toward the bedding plane is more significant as the perforating phase angle becomes larger. For the damage mechanism, when $\beta = 0°$, fracture propagation is mainly due to the effect of tensile damage of the bedding plane. When $\beta = 90°$, the fracture propagation is mainly due to the effect of tensile damage of the matrix. The stress concentration at the perforating tip competes with the shear action of the weak bedding plane resulting in different degrees of fracture deflection (Wang et al., 2022).

Table 2
Mechanical parameters of different rock matrices.

Rock matrices	Young's modulus, GPa		Poisson's ratio		Critical energy release rate, N/m		Layer
Isotropic	E 15.2		v 0.26		G_c 80.56		n /
Transversely isotropic	E_1 21.1	E_2 15.2	v_{12} 0.19	v_{23} 0.26	G_{c1} 14.63	G_{c2} 80.56	n /
Multilayer isotropic	E_1 15.2	E_2 5.5	v_1 0.26	v_2 0.26	G_{c1} 80.56	G_{c2} 29.15	n 80

where E - GPa, v, G_c - N/m represent Young's modulus, Poisson's ratio and critical energy release rate of different rock matrices, n represents the number of shale layers.

3.2. Influence of perforating phase angle on energy for fracture propagation

Fig. 10(a) shows the pressure-time curves of shale with different

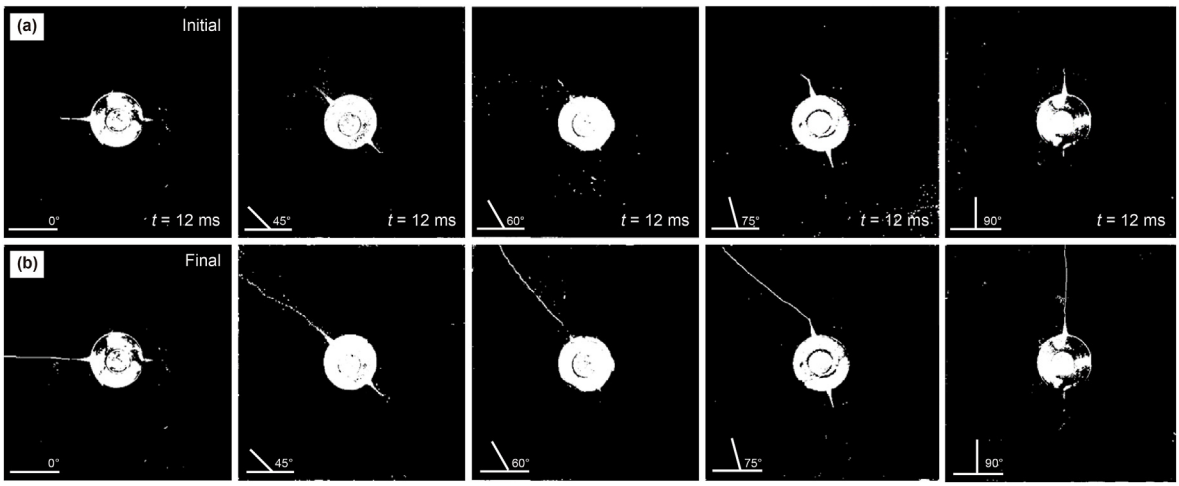

Fig. 8. Initial (**a**) and final (**b**) propagation morphology of five shale samples.

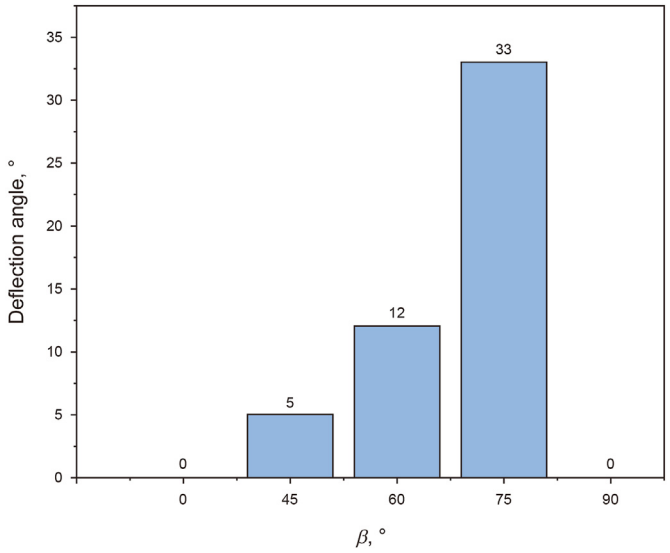

Fig. 9. Deflection angles during propagation of five shale samples.

perforating phase angles. When the load reaches the peak value, the load-time curve drops instantaneously. This load-time curve trend indicates its internal brittle fracture is dominant during the loading failure of shale, thus showing strong brittle nature.

Fig. 10(b) shows the slope of different shale pump pressure curves during the decline phase. The results show that when $\beta = 0°$, the curve slope becomes the minimum. On the contrary, the curve slope becomes the maximum when $\beta = 90°$. The difference in tensile strength between the matrix and the weak bedding plane is the main reason (Shi et al., 2022). When $\beta = 45°$, 60°, and 75°, the slope of the curve is decreasing. It indicates that the different perforating phase angles lead to anisotropy in the tensile strength of shale which in turn causes the energy required for hydraulic fractures to propagate in the shale to vary.

Fig. 11(a) shows the fracture propagation rate of shale samples at different times for five different perforating phase angles. Fig. 11(b) shows the initiation pressure of five shale samples at different perforating phase angles. It is noted that the initiation pressure corresponds to the fracture propagation rate. The results show that when $\beta = 0°$, the fracture propagation rate becomes the maximum and the initiation pressure becomes the minimum. On the contrary, the fracture propagation rate becomes the minimum and the initiation pressure becomes the maximum when $\beta = 90°$. It indicates that $\beta = 0°$ is more likely to cause hydraulic fracture propagation than $\beta = 90°$. When $\beta = 0°$, the perforating phase is aligned with the bedding plane direction, the synergistic interaction between the perforating phase and the weak bedding plane makes it easier for the fracture to propagate along this angle, so fracture propagation requires less energy. When $\beta = 90°$, the fracture propagates along the perforating phase and the perforation plays a dominant role. Fracture penetrates the shale matrix and

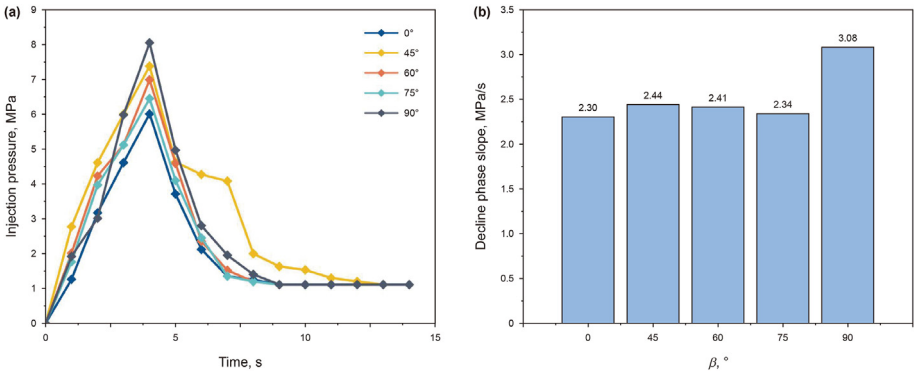

Fig. 10. Injection pressure profile (**a**) and the slope of pump pressure curves during the decline phase (**b**) of five shale samples.

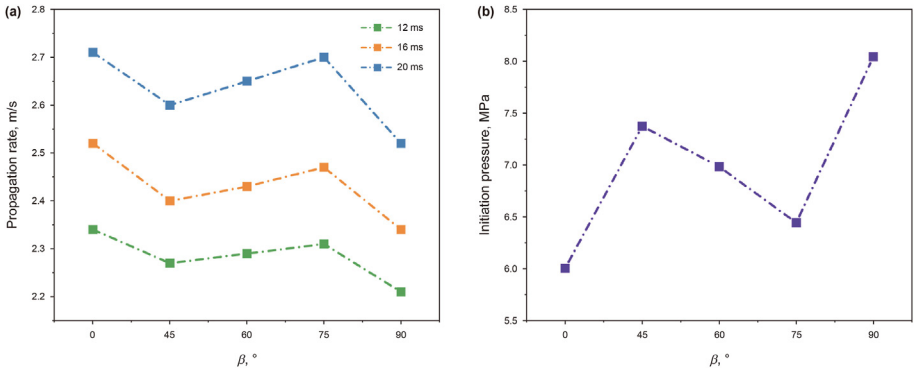

Fig. 11. The fracturing behavior of five test samples: (**a**) the fracture propagation rate; (**b**) fracture initiation pressure.

requires high energy to break the matrix (Heng et al., 2021). Furthermore, when $\beta = 45°$, 60°, and 75°, the fracture propagation rate increases gradually as the perforating phase angle becomes larger and initiation pressure decreases gradually as the perforating phase angle increases. It indicates that the bedding plane and the perforating phase compete with each other and the dominant role of the bedding plane increases with the increase of perforating phase angle, so the energy required for fracture propagation decreases with the increase of perforating phase angle.

3.3. Influence of shale medium characteristics on fracture propagation

In this section the above experiments were implemented through a 2D numerical model of fracture propagation under fluid-structure coupling for a better understanding of the fracture propagation mechanism under different perforating phases. Fig. 12 shows the numerical simulation results in three different rock matrices under the same experimental conditions ($\beta = 60°$). It can be observed that the fractures in isotropic rock matrix propagated exactly in the direction of the perforating phase. In the transversely isotropic rock matrix, the fracture morphology is observed to be fully affected by the weak bedding plane and propagated along the direction of e_2 which has the maximum critical energy release rate G_{c2}. Fig. 13 shows the fluid pressure field of three different rock matrices ($\beta = 60°$). It is observed that the fluid pressure field has a consistent shape with the phase field, and the fluid pressure has a maximum value in the fracture domain. Fig. 14 shows the effective maximum stress distributions of three different rock matrices ($\beta = 60°$). The stress distributions coincide with the fracture patterns and the stress concentration is observed only around the fracture tip (Zhuang et al., 2020).

Since shale have obvious bedding structure, it is mostly studied as transversely isotropic (Tan et al., 2021; Zhang et al., 2021). However, the numerical simulation results of isotropic and transversely isotropic are quite different from the experimental results. Therefore, we speculate that the existence of bedding planes may not be completely equivalent to transversely isotropic. So, the rock matrix was divided into multiple layers of isotropic medium superimposed while the layers were tightly connected. The conjecture was verified by changing the mechanical parameters of the thin layers to reflect the differences between the shale layers. The comparison between numerical simulation and experimental results further confirms the competitive relationship between

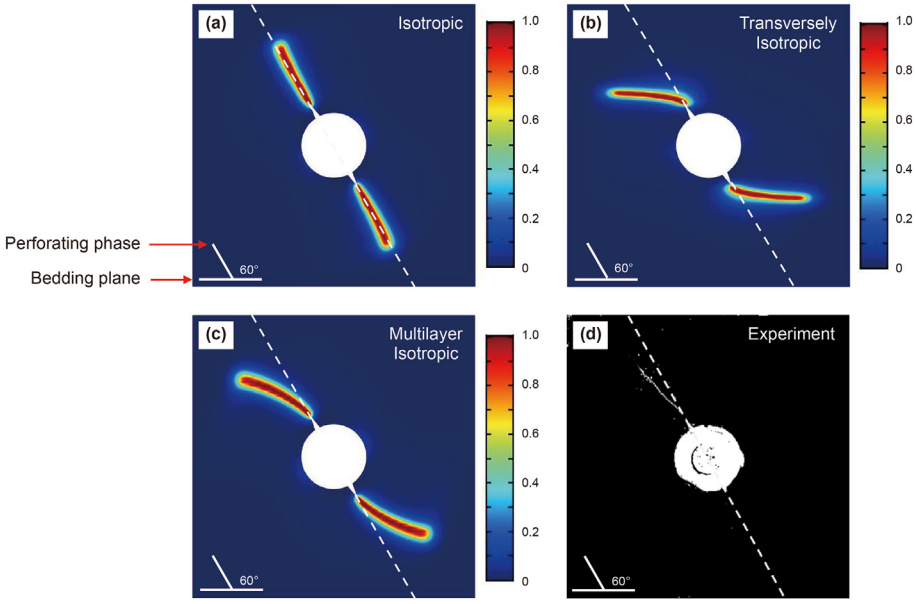

Fig. 12. Comparison of numerical simulation results of hydraulic fracture propagation in (**a**) isotropic rock matrix, (**b**) transversely isotropic rock matrix, (**c**) multilayer rock matrix and (**d**) experimental results.

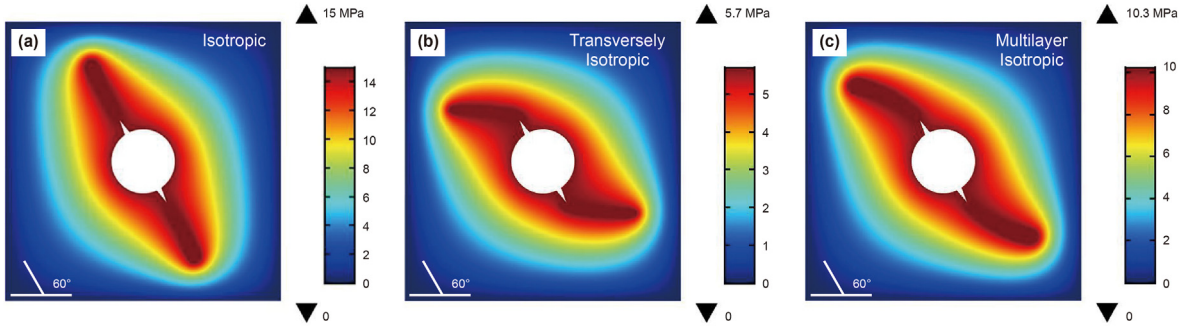

Fig. 13. Fluid pressure field of hydraulic fracture propagation in (**a**) isotropic rock matrix, (**b**) transversely isotropic rock matrix and (**c**) multilayer rock matrix.

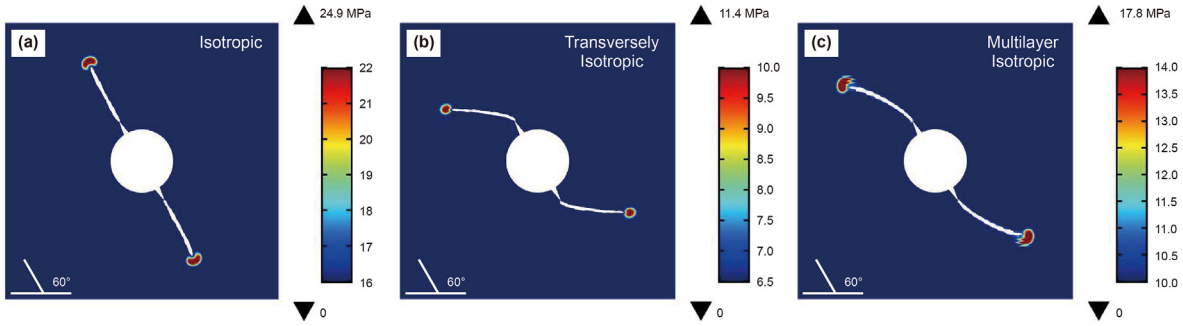

Fig. 14. Effective maximum stress distributions in (**a**) isotropic rock matrix, (**b**) transversely isotropic rock matrix and (**c**) multilayer rock matrix.

perforating phase and bedding planes on fracture propagation.

3.4. Discussion

The influences of perforating phase and bedding planes on the fracture deflection in laminated shale have been studied, evaluated and cross validated in this study. It can be observed from the fracture propagation trajectories, see Fig. 8, that the stress concentration of the mode I fracture and the shear interaction of the weak bedding plane lead to the fracture deflection in different degrees during the propagation. When $\beta = 0°$ and 90°, the fracture propagations are mainly related to the tensile failure, which is mode I fracture (Lash and Engelder, 2005). When $\beta = 45°$, 60°, and 75°, the fracture propagations are mainly related to the tensile-shear failure, which is mode I-II fracture (Erarslan and Williams, 2013).

Perforating phase angle impacts not only the failure modes but also the energy required for fracture propagation. The data of initiation pressure and propagation rate of shale in different perforating phases reveal that the energy required along the bedding plane is significantly less than that in the matrix. It is consistent with the experimental conclusions obtained by Luo et al. (2018) and Sedman et al. (2012). Furthermore, with the increase of fracture initiation pressure, more energy is required and the propagation rate becomes slower.

The numerical simulation results in different rock matrices explain the internal cause for the different degrees of fracture deflection. As shown in Fig. 15, the fracture propagation trajectories of isotropic and transversely isotropic are quite different from the experimental results. This is due to the materials used in the simulation are strictly transversely isotropic but the shale used in the experiment does not fully comply with the transversely isotropic assumption but only between the layers. Natural shale is composed of multilayers of isotropic medium which is transversely

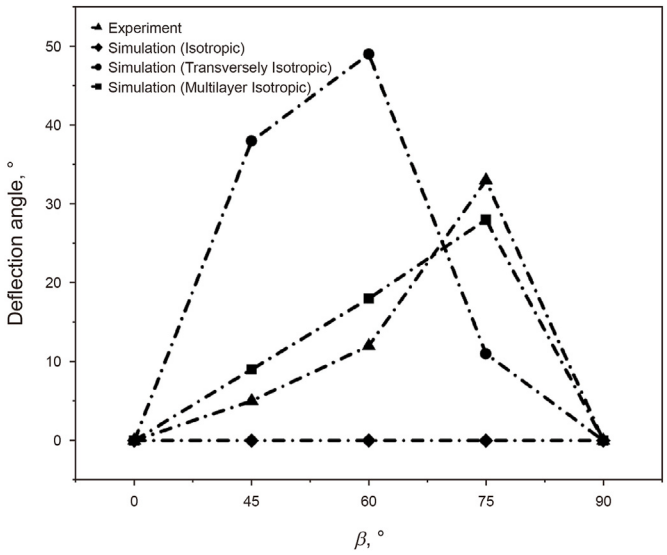

Fig. 15. Comparison of fracture deflection angles under different conditions.

isotropic in macroscopic view. Therefore, the numerical model was furtherly refined and verified the above conjecture. In terms of fracture propagation, the existence of shale bedding plane is not exactly equivalent to anisotropy but to the accumulation of multiple different homogeneous layered structures. Shale is not strictly transversely isotropic material but is intermediate between isotropic and transversely isotropic media in some ways. The complexity of shale mechanics will affect the hydraulic fracturing mode and lead to the complex fracture network in the formation (Hu et al., 2021; Khan et al., 2023).

4. Conclusions

This paper proposed a 2D laboratory imaging scheme for hydraulic fracturing test to study the competition effects on fracture propagation between perforating phase and bedding planes. In addition to original images of fracture evolution, phase field models were used to gain further insight into the fracture propagations that generate hydraulic fracture complexity. It can be concluded the following four parts:

(1) Fracture propagation behavior is controlled by perforating phase and bedding planes, which are mutually competitive. The fractures penetrate into the matrix and the bedding planes appear to be no influence on fracture propagation when the perforating phase is perpendicular to the bedding planes. When the perforating phase angle is relatively small, the effect of perforating phase on fracture propagation deflection is weakened and bedding planes plays a dominant role. In particular, the fracture propagation deflection is largest when the perforating phase is the angle 75° of bedding planes.
(2) The variations in bedding and matrix strength lead to a regular influence of perforating phase angle on the energy required for fracture propagation. The maximum energy is required when the perforating phase is perpendicular to the bedding planes. Conversely, the minimum energy is required when the perforating phase aligns with the bedding planes. In addition, when the perforating phase is the angle 45°, 60°, and 75° of bedding planes, the energy required decreases with the increase of perforating phase angle.
(3) The intrinsic characteristics of shale is manifested in the mechanical difference between the shale layers. The transversely isotropic assumption is not sufficient to characterize the nature of shale. The difference in mechanical properties between different shale layers is the fundamental reason for different fracture deflections.
(4) There are two aspects of limitation in this study involving the sample scale issues and in-situ stress. Because of the size limitation, the effective propagation paths of fractures without boundary effects are relatively short. The in-situ stress definitely affects on the fracture propagation. The extended work will take account into the factor of in-situ stress.

CRediT authorship contribution statement

Ming-Zhe Gu: Conceptualization, Data curation, Investigation, Methodology, Writing – original draft, Writing – review & editing. **Mao Sheng:** Funding acquisition, Methodology, Project administration, Resources, Supervision, Writing – review & editing. **Xiao-Ying Zhuang:** Formal analysis, Methodology, Resources, Software, Supervision, Writing – review & editing. **Xin-Yi Li:** Investigation, Methodology, Software, Writing – original draft. **Gen-Sheng Li:** Project administration, Resources, Supervision.

Declaration of competing interest

The authors declare that they have no known competing financial interests or personal relationships that could have appeared to influence the work reported in this paper.

Acknowledgments

This work was financially supported by the National Natural Science Foundation of China (Grant Nos.52074315 & U19B6003).

Appendix

Table A1
Uniaxial compression test data

Sample identifier	Direction	Failure strength, MPa	Young's modulus, GPa	Poisson's ratio
P-1	Parallel	83.0	22.0	0.21
P-2		73.0	22.9	0.18
P-3		102.0	18.3	0.18
C-1	Vertical	66.0	14.4	0.27
C-2		47.6	17.3	0.29
C-3		63.8	13.8	0.22

Table A2
Propagation regimes of shale hydraulic fractures

Test	Q_0	μ, mPa·s	lgτ	Regime
Our experiment	20 mL/min	1	6.428	Toughness
Bunger (2008)	12 mL/min	80	2.483	Viscosity
Lu et al. (2022)	0.2 mL/min	110	6.373	Toughness
Shale-1	5 m^3/min	40	−4.582	Viscosity
Shale-2	1 m^3/min	1	6.419	Toughness

where τ represents the dimensionless parameter of fracture evolution.

References

Abass, H.H., Hedayati, S., Meadows, D., 1996. Nonplanar fracture propagation from a horizontal wellbore: experimental study. SPE Prod. Facil. 11 (3), 133–137. https://doi.org/10.2118/24823-PA.
Bai, Q., Liu, Z., Zhang, C., et al., 2020. Geometry nature of hydraulic fracture propagation from oriented perforations and implications for directional hydraulic fracturing. Comput. Geotech. 125, 103682. https://doi.org/10.1016/j.compgeo.2020.103682.
Bunger, A.P., Detournay, E., 2008. Experimental validation of the tip asymptotics for a fluid-driven crack. J. Mech. Phys. Solid. 56 (11), 3101–3115. https://doi.org/10.1016/j.jmps.2008.08.006.
Cai, C., Wang, X., Yuan, X., et al., 2019. Experimental investigation on perforation of shale with ultra-high pressure abrasive water jet: shape, mechanism and sensitivity. J. Nat. Gas Sci. Eng. 67, 196–213. https://doi.org/10.1016/j.jngse.2019.05.002.
Cong, Z., Li, Y., Tang, J., et al., 2022. Numerical simulation of hydraulic fracture height layer-through propagation based on three-dimensional lattice method. Eng. Fract. Mech. 264, 108331. https://doi.org/10.1016/j.engfracmech.2022.108331.
Daneshy, A.A., 1973. Experimental investigation of hydraulic fracturing through perforations. J. Petrol. Technol. 25 (10), 1201–1206. https://doi.org/10.2118/4333-PA.
Daneshy, A.A., 2003. Off-balance growth: a new concept in hydraulic fracturing. J. Petrol. Technol. 55 (4), 78–85. https://doi.org/10.2118/80992-JPT.
Detournay, E., 2016. Mechanics of hydraulic fractures. Annu. Rev. Fluid Mech. 48, 311–339. https://doi.org/10.1146/annurev-fluid-010814-014736.

Erarslan, N., Williams, D., 2013. Mixed-mode fracturing of rocks under static and cyclic loading. Rock Mech. Rock Eng. 46, 1035–1052. https://doi.org/10.1007/s00603-012-0303-5.
Francfort, G.A., Marigo, J.J., 1998. Revisiting brittle fracture as an energy minimization problem. J. Mech. Phys. Solid. 46 (8), 1319–1342. https://doi.org/10.1016/S0022-5096(98)00034-9.
Guo, T., Zhang, S., Qu, Z., et al., 2014. Experimental study of hydraulic fracturing for shale by stimulated reservoir volume. Fuel 128, 373–380. https://doi.org/10.1016/j.fuel.2014.03.029.
He, J., Zhang, K., Liu, H., et al., 2022. Laboratory investigation on hydraulic fracture propagation in sandstone-mudstone-shale layers. Petrol. Sci. 19 (4), 1664–1673. https://doi.org/10.1016/j.petsci.2022.03.018.
Heng, S., Li, X., Zhang, X., et al., 2021. Mechanisms for the control of the complex propagation behaviour of hydraulic fractures in shale. J. Petrol. Sci. Eng. 200, 108417. https://doi.org/10.1016/j.petrol.2021.108417.
Hou, B., Zhang, R., Zeng, Y., et al., 2018. Analysis of hydraulic fracture initiation and propagation in deep shale formation with high horizontal stress difference. J. Petrol. Sci. Eng. 170, 231–243. https://doi.org/10.1016/j.petrol.2018.06.060.
Hu, Y., Wang, Q., Zhao, J., et al., 2021. Numerical simulation of complex fracture geometry caused by hydrodynamics in shale with pre-existing weak planes. J. Petrol. Sci. Eng. 199, 108306. https://doi.org/10.1016/j.petrol.2020.108306.
Khan, J.A., Padmanabhan, E., Haq, I.U., et al., 2023. Hydraulic fracturing with low and high viscous injection mediums to investigate net fracture pressure and fracture network in shale of different brittleness index. Geomechanics for Energy and the Environment 33, 100416. https://doi.org/10.1016/j.gete.2022.100416.
Lash, G.G., Engelder, T., 2005. An analysis of horizontal microcracking during catagenesis: example from the Catskill delta complex. AAPG (Am. Assoc. Pet. Geol.) Bull. 89 (11), 1433–1449. https://doi.org/10.1306/05250504141.
Lei, X., Zhang, S., Xu, G., et al., 2015. Impact of perforation on hydraulic fracture initiation and extension in tight natural gas reservoirs. Energy Technol. 3 (6), 618–624. https://doi.org/10.1002/ente.201402206.
Li, C., Xie, L., Ren, L., et al., 2013. Evaluating the applicability of fracture criteria to predict the crack evolution path of dolomite based on SCB experiments and FEM. Math. Probl Eng., 959806 https://doi.org/10.1155/2013/959806.
Liu, J., Liang, X., Xue, Y., et al., 2020. Investigation on crack initiation and propagation in hydraulic fracturing of bedded shale by hybrid phase-field modeling. Theor. Appl. Fract. Mech. 108, 102651. https://doi.org/10.1016/j.tafmec.2020.102651.
Liu, Z., Jin, Y., Chen, M., et al., 2016. Analysis of non-planar multi-fracture propagation from layered-formation inclined-well hydraulic fracturing. Rock Mech. Rock Eng. 49, 1747–1758. https://doi.org/10.1007/s00603-015-0872-1.
Lu, G., Momeni, S., Lecampion, B., 2022. Experimental investigation of hydraulic fracture growth in an anisotropic rock with pre-existing discontinuities under different propagation regimes. In: ARMA US Rock Mechanics/Geomechanics Symposium. 26–29, June,. https://doi.org/10.56952/ARMA-2022-0239. Santa Fe, New Mexico.
Luo, Y., Xie, H., Ren, L., et al., 2018. Linear elastic fracture mechanics characterization of an anisotropic shale. Sci. Rep. 8 (1), 1–12. https://doi.org/10.1038/s41598-018-26846-y.
Michael, A., Gupta, I., 2020. Analytical orientation criteria for drilling and completion-induced fracture initiation considering fluid infiltration from the wellbore. J. Petrol. Sci. Eng. 190, 107033. https://doi.org/10.1016/j.petrol.2020.107033.
Sedman, A., Talviste, P., Mõtlep, R., et al., 2012. Geotechnical characterization of Estonian oil shale semi-coke deposits with prime emphasis on their shear strength. Eng. Geol. 131, 37–44. https://doi.org/10.1016/j.enggeo.2012.02.002.
Shi, X., Zhao, Y., Danesh, N.N., et al., 2022. Role of bedding plane in the relationship between Mode-I fracture toughness and tensile strength of shale. Bull. Eng. Geol. Environ. 81 (2), 81. https://doi.org/10.1007/s10064-022-02572-8.
Tan, P., Jin, Y., Pang, H., 2021. Hydraulic fracture vertical propagation behavior in transversely isotropic layered shale formation with transition zone using XFEM-based CZM method. Eng. Fract. Mech. 248, 107707. https://doi.org/10.1016/j.engfracmech.2021.107707.
Wang, X., Zhu, Z., Zhou, L., et al., 2022. Study on the effects of joints orientation and strength on failure behavior in shale specimen under impact loads. Int. J. Impact Eng. 163, 104162. https://doi.org/10.1016/j.ijimpeng.2022.104162.
Wang, Y., Hou, B., Wang, D., et al., 2021. Features of fracture height propagation in cross-layer fracturing of shale oil reservoirs. Petrol. Explor. Dev. 48 (2), 469–479. https://doi.org/10.1016/S1876-3804(21)60038-1.
Wu, S., Ge, H., Li, T., et al., 2022. Characteristics of fractures stimulated by supercritical carbon dioxide fracturing in shale based on acoustic emission monitoring. Int. J. Rock Mech. Min. Sci. 152, 105065. https://doi.org/10.1016/j.ijrmms.2022.105065.
Zhang, J., Yu, H., Wang, Q., et al., 2022. Hydraulic fracture propagation at weak interfaces between contrasting layers in shale using XFEM with energy-based criterion. J. Nat. Gas Sci. Eng. 101, 104502. https://doi.org/10.1016/j.jngse.2022.104502.
Zhang, J., Yu, Q., Li, Y., et al., 2023. Hydraulic fracture vertical propagation mechanism in interlayered brittle shale formations: an experimental investigation. Rock Mech. Rock Eng. 56 (1), 199–220. https://doi.org/10.1007/s00603-022-03094-1.
Zhang, M., Fan, X., Zhang, Q., et al., 2021. Parametric sensitivity study of wellbore stability in transversely isotropic medium based on polyaxial strength criteria. J. Petrol. Sci. Eng. 197, 108078. https://doi.org/10.1016/j.petrol.2020.108078.
Zhang, R., Hou, B., Shan, Q., et al., 2018. Hydraulic fracturing initiation and near-wellbore nonplanar propagation from horizontal perforated boreholes in tight formation. J. Nat. Gas Sci. Eng. 55, 337–349. https://doi.org/10.1016/j.jngse.2018.05.021.
Zhou, S., Zhuang, X., 2020. Phase field modeling of hydraulic fracture propagation in transversely isotropic poroelastic media. Acta Geotechnica 15 (9), 2599–2618. https://doi.org/10.1007/s11440-020-00913-z.
Zhou, S., Zhuang, X., Rabczuk, T., 2018. A phase-field modeling approach of fracture propagation in poroelastic media. Eng. Geol. 240, 189–203. https://doi.org/10.1016/j.enggeo.2018.04.008.
Zhuang, X., Li, X., Zhou, S., 2023. Three-dimensional phase field feature of longitudinal hydraulic fracture propagation in naturally layered rocks under stress boundaries. Eng. Comput. 39 (1), 711–734. https://doi.org/10.1007/s00366-022-01664-z.
Zhuang, X., Zhou, S., Sheng, M., et al., 2020. On the hydraulic fracturing in naturally-layered porous media using the phase field method. Eng. Geol. 266, 105306. https://doi.org/10.1016/j.enggeo.2019.105306.
Zou, J., Chen, W., Jiao, Y., 2018. Numerical simulation of hydraulic fracture initialization and deflection in anisotropic unconventional gas reservoirs using XFEM. J. Nat. Gas Sci. Eng. 55, 466–475. https://doi.org/10.1016/j.jngse.2018.04.033.